

## Article

# Role of Electronic and Steric Effects on Ruthenium Catalysts with Bulky NHC Ligands and Relationship with the Z-Selectivity in Olefin Metathesis

Valentina Diaz-González<sup>1</sup> and Katherine Paredes-Gil<sup>1,2,\*</sup> 

<sup>1</sup> Departamento de Química, Facultad de Ciencias Naturales, Matemática y del Medio Ambiente, Universidad Tecnológica Metropolitana, Santiago 7800003, Chile; vdiazgo@utem.cl

<sup>2</sup> Programa Institucional de Fomento a la Investigación, Desarrollo e Innovación, Universidad Tecnológica Metropolitana, Ignacio Valdivieso 2409, San Joaquín, Santiago 8940577, Chile

\* Correspondence: k.paredesg@utem.cl

**Abstract:** Recently, sterically demanding N-heterocyclic cyclometalated ruthenium were reported as efficient Z-selective catalysts for cross-metathesis, showing a different reactivity in the function of the auxiliary ligand and the bulky ligand. To understand the origin of this behavior, we carried out density functional (M06-L) calculations to explore the reaction mechanism and insight from the energetic contributions into the determinant step. We emphasize the differences that occur when the 2,6-diisopropylphenyl (Dipp) and 2,6-diisopentylphenyl (Dipep) are employed. The results show that the barrier energies,  $\Delta G^\ddagger$ , increase when the bulky ligand is greater, using nitrate as an auxiliary ligand, while the opposite behavior is obtained when pivalate is the auxiliary ligand. This tendency has its origin in the low reorganization energy and the less steric hindrance ( $\%V_{\text{bur}}$ ) obtained in catalysts that involve nitrate ligand and Dipep group. Moreover, by scrutinizing the energy decomposition analysis (EDA), it is found that the electronic contributions are also dominant and are not uniquely the steric effects that control the Z-selectivity.

**Keywords:** density functional theory; cross metathesis; Z-selectivity; steric and electronic effects



**Citation:** Diaz-González, V.; Paredes-Gil, K. Role of Electronic and Steric Effects on Ruthenium Catalysts with Bulky NHC Ligands and Relationship with the Z-Selectivity in Olefin Metathesis. *Catalysts* **2023**, *13*, 1305. <https://doi.org/10.3390/catal13091305>

Academic Editors: Maria Luisa Di Gioia, Luisa Margarida Martins and Isidro M. Pastor

Received: 24 August 2023

Revised: 7 September 2023

Accepted: 12 September 2023

Published: 19 September 2023



**Copyright:** © 2023 by the authors. Licensee MDPI, Basel, Switzerland. This article is an open access article distributed under the terms and conditions of the Creative Commons Attribution (CC BY) license (<https://creativecommons.org/licenses/by/4.0/>).

## 1. Introduction

Olefin metathesis is a methodology that transforms carbon–carbon double bonds into valuable molecules with application in green chemistry [1,2], biochemistry [3,4], and materials science [4,5], among others [6]. Cross-metathesis (CM), Ring Closing Metathesis (RCM), and Ring Opening Metathesis Polymerization (ROMP) are outstanding in industrial processes [6,7]. These reactions are mediated by Ru, Mo-, V-, and W-based carbene-type catalysts [8–11]. CM is an equilibrium process between two terminal alkenes, giving rise to a mixture of olefins with trans- (*E*) or cis- (*Z*) isomerism (Figure 1a). In general, first- (Grubbs 1st), second- (Grubbs 2nd), and Hoveyda–Grubbs (1st and 2nd) catalysts are thermodynamic, favoring *E*-selectivity [12]. In 2012, Keitz designed a new catalyst with an asymmetric and bulky ligand, 1-adamantyl (Adm), an O-bidentate anionic group such as substituted carboxylate (Ru-1), and a lateral arm of the N-heterocyclic carbene (NHC), 2,6-diisopropylphenyl group (Mes). This was the first example of a Ru-based catalyst with high Z-selectivity in cross-metathesis reactions (>95%) [13]. This breakthrough prompted researchers to create new catalytic systems that access a Z-preference over the *E*-preference [14–16].

Other Keitz's results showed higher activity and stability compared with substituted carboxylate when the anionic group is substituted by nitrate (Ru-2) [17]. Several attempts to improve the catalytic activity, selectivity, and stability have been realized through the design of new catalysts such as those described in Figure 2. For instance, the substitution of the O-bidentate by an S-bidentate anionic group, catechol type, (Ru-3) [18] and the

chlorine addition to the catechol group (Ru-4) [19], both without the bulky ligand Adm, gave origin to catalysts with high selectivity (>98%) in the CM of allylic alcohols. Also, it is important to highlight the challenging proposal to include chelating laterals with a smaller volume than the Adm group (Ru-5) [20]. Recently, the ab initio design proposed and synthesized the first S-monodentate catalyst (Ru-6) [21], reaching up to 80% in prototypical homocoupling metathesis reactions. Thus, the nature of the anionic group, different electron acceptor residues, and the size of the chelate ligand would influence the origin of the Z-selectivity, suggesting that the steric effect is not uniquely responsible.

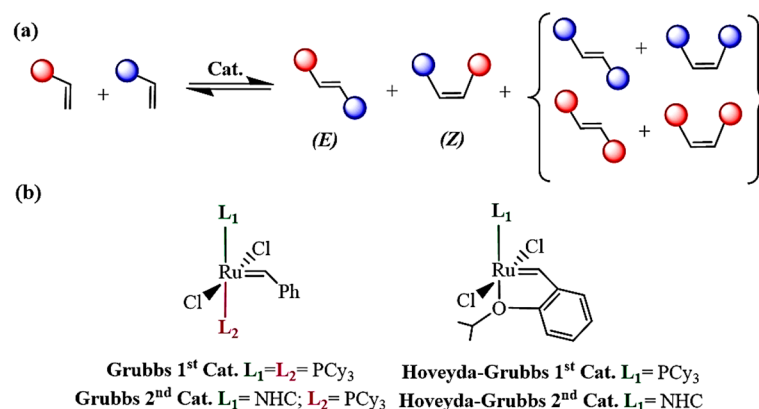


**Figure 1.** (a) Scheme of cross-metathesis reaction, (b) Classical Grubbs generations catalysts.

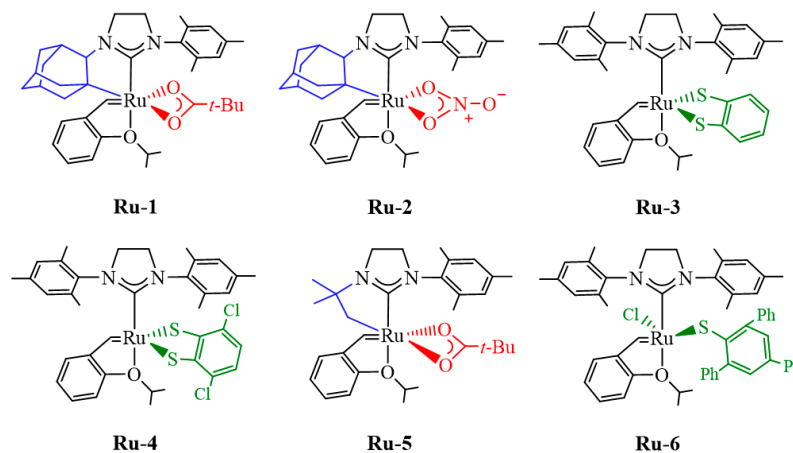


**Figure 2.** Ruthenium catalysts potentially active in Z-selectivity.

Recently, Grubbs reported the preparation of sterically demanding N-heterocyclic cyclometalated ruthenium catalysts with applications in CM between acrylamides and terminal olefins [22]. Historically, the acrylamide–olefin metathesis reaction (Figure 3a) using Ru-1 and Ru-2 was difficult due to the high thermodynamic stability towards E-selectivity (>25:1) and the long reaction times exceeding 48 h [23]. To overcome this difficulty, proposed catalysts were derived from the incorporation of an even bulkier N-substituent than the Mes, such as the 2,6-diisopropylphenyl (Dipp) [24,25] and 2,6-diisopentylphenyl (Dipep) [26] groups, as is described in Figure 3b for the complexes Ru-7 to Ru-8 and Ru-9 to Ru-10, respectively. In this work, when Ru-7 was employed, a Z-amide and Z-olefin were obtained with a yield of 27% and 63%, respectively; if the anionic group was exchanged to carboxylate (Ru-8), the yield increased remarkably up to 49% to the Z-amide and decreased to 11% to the olefin. In turn, this limit was exceeded by the Ru-10 system, which produced the maximum yield (80%) for Z-amide and a new increase of 27% for Z-olefin. Thus, the reactivity of the CM can be significantly influenced by the combination of the auxiliary ligand nature and the bulkier N-substituent NHC ligand.

Hence, gaining knowledge of these contributions can facilitate a broader comprehension of olefin metathesis.

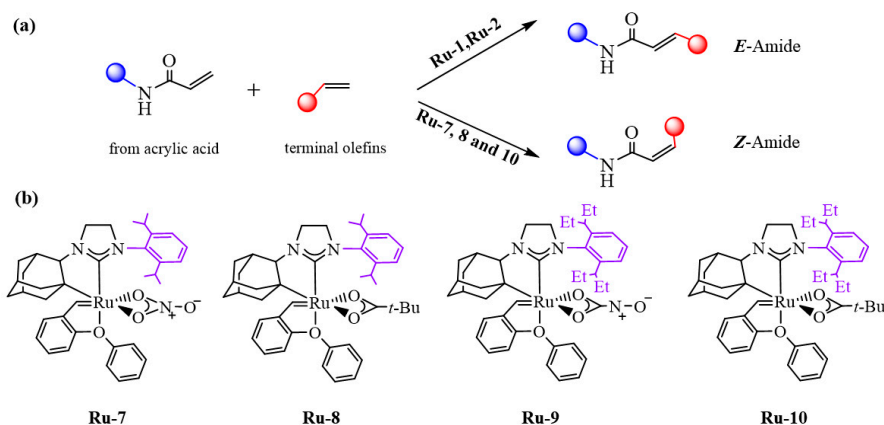


**Figure 3.** (a) The acrylamide–olefin cross-metathesis with Z-selectivity, (b) Sterically demanding N-heterocyclic with Dipp and Dipep cyclometalated ruthenium catalysts.

The experimental and theoretical description of the reaction mechanism in olefin metathesis has been a challenge [27–33]. The generally accepted mechanism, depicted in Figure 4, begins with the activation of the 16-electron pre-catalyst through the dissociation reaction of the Ru–O bond originating from the isopropyl, resulting in the formation of a 14-electron Ru-alkylidene active intermediate (14-Int).

The formation of the active intermediate gives rise to the next stage, which entails the coordination of the olefinic substrate in two coordination modes: a) *trans* to NHC (called *bottom* pathway or b) *trans* to bidentate anionic group (called *side* pathway). In both pathways, metallocyclobutane (MC) is produced as a result of [2+2] cycloaddition (TSCA) being surmounted. In the following step of the isomerization of the MC intermediate, a [2+2] cycloreversion (TSCR) gives rise to the decooordination of the new olefin. These pathways are crucial for the *E*-/*Z*-selectivity. If methyl substituents are located behind (B) or in front of (F) to the metallocycle plane on the *bottom* pathway, an *E*-2-butene olefin is obtained, whereas if they are located up (U) and down (D) on the *side* pathway, a *Z*-2-butene alkene is produced. Figure 4 depicts the main transition states of each substage, along with their respective abbreviation.

The origin of *Z*-selectivity in olefin metathesis has been the focus of a variety of studies in recent years. In this field, Liu [32] reported that the *side* preference for Ru-1 can be explained by steric and electronic factors of the different ligands that influence the metal center's stability. According to the results, the *cis* products are driven by the *side* mechanism due to a kinetic preference. The Gibbs energy difference between the most favorable mechanism (*side*) and the less favorable pathway (*bottom*) was reported at 10.4 kcal/mol ( $\Delta\Delta G_{\text{Bottom-Side}}$ ). Within this mechanism, the substituents originating from the olefin acquire a spatial orientation opposite to that of the bulky Mes. In terms of the electronic effect, the transition states of the "*bottom*" mechanism are destabilized due to the back-donation from  $\pi^*$  orbitals of both NHC and alkylidene to two different types of d orbitals on Ruthenium, whereas in the "*side*" mechanism, the retro donation involves the same d orbital, resulting in the stability. Wang and Dang [34] found comparable results for Ru-2.

In addition, Hoveyda and co-workers have conducted an analysis of other catalysts, such as the Ru-3 [18]. The researchers studied four possible reaction pathways, including styrene as substrate, and determined the steric effect by analyzing the spatial orientation of the carbene substituent in relation to the NHC. In the most favorable pathway, the geometry of the transition state for the [2+2] cycloaddition reveals that the Ru carbene substituent is oriented away from the NHC, exhibiting a barrier of 3.2 kcal/mol. During the exploration of the subsequent, more stable route, a steric hindrance between the species was identified,

with an energetic value of 6.4 kcal/mol. Therefore, this work highlighted that the presence of a significant steric repulsion in the metallocycle plays a crucial role in promoting the preferential formation of *Z*-selectivity.

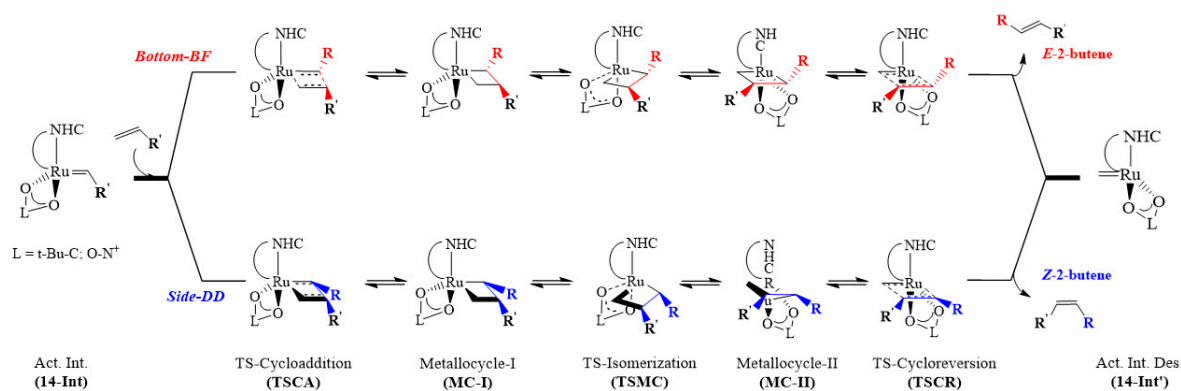


**Figure 4.** *Bottom* and *Side* pathways for olefin metathesis with ruthenium NHC catalysts using propene as initiating alkene [32,35,36].

Also, a modified Ru-3 catalyst [37] with Dipp ligand was analyzed, suggesting that this substituent would lead to a greater steric effect, thereby favoring a suitable spatial position in the MCy for *Z*-selectivity. Martinez [38] studied the initial stage of the Ru-3 and ethylene-based olefin metathesis to delve deeper into this subject. In the initial stage, by altering the dihedral angle around styrene, eight structures with distinct positions and orientations were discovered. The energetic values of the structures evaluated in the initiation stage range from 0 to 22 kcal/mol.

The most important result is the dissociation Ru-S bond, which suggests that the S-monodentate promotes the subsequent stages of olefin metathesis. In the mechanism, they evaluated *bottom* and *side* pathways and quantified the steric and electronic properties using the activation strain model. They discovered that the *Z*-isomer can be formed by kinetic control and suggest that the metallocycle can be stabilized by the electronic effect of the active species and a reduction in the olefin's strain. These works demonstrate the relevance of understanding the factors that govern *Z*-selectivity in olefin metathesis.

As a result of these findings, it is essential to identify, comprehend, and investigate the steric and electronic effects that control the *Z*-selectivity in ruthenium catalysts. Experiments have shown that changing the auxiliary ligand and increasing the steric volume around the central may have a considerable impact on selectivity [22]. In this direction, we explore the ethane cross-metathesis reaction mechanism and understand the energetic contributions (steric and electronic) to the rate-determining step, emphasizing the differences between 2,6-diisopropylphenyl (Dipp) and 2,6-diisopentylphenyl (Dipep). Therefore, the dominance of steric-electronic factors in the activation energies of the *Z*-selective represents a new limit to be overcome, allowing advancement in the design of more specialized catalysts.

## 2. Results

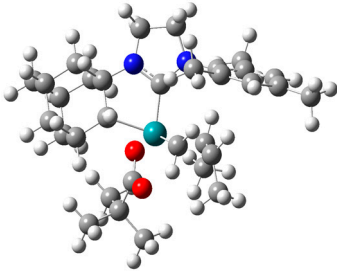
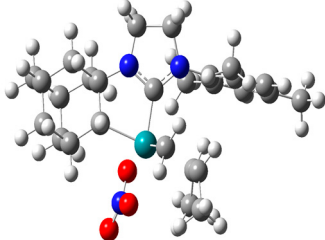
### 2.1. Bottom and Side Mechanism Employing the Keitz–Grubbs-Substituted, Ru-1 and Ru-2 Catalysts

Figures S1 and S2 depict the energy profiles for the CM reaction with Ru-1 and Ru-2 catalysts, respectively. In both instances, the *Side-DD* pathway is observed to be more stable than the *Bottom-BF*. The limiting stage or Ru-1 is the TSCR with barrier energies of 20.3 kcal/mol and 32.4 kcal/mol, respectively. Consequently, the barrier Gibbs energy  $\Delta\Delta G_{Bottom-Side}$  difference for Ru-1 and Ru-2 are 12.1 kcal/mol and 18.4 kcal/mol, respectively. Thus, our methodology can reproduce the main *Z*-product formation in these catalysts as observed experimentally. In addition, these results are consistent with the energy gap  $\Delta\Delta G_{Bottom-Side}$  closest to 10 kcal/mol obtained by Liu et al., [32] which demon-

states that a kinetic control is essential for *Z*-selectivity. Figures S3 and S4 depict the optimized intermediate and transition structures for the *side* pathway of each catalyst.

In addition, an energy decomposition analysis (EDA) was conducted. Table 1 describes the reorganization and interaction contribution energies of the limiting stages for Ru-1 and Ru-2. In general, the reorganization contribution ( $\Delta E_{reorg\ t}$ ) in Ru-1 is significantly higher in *Bottom-BF* than *Side-DD*, with respective values of 50.9 kcal/mol and 41.5 kcal/mol. Similar results were discovered for Ru-2. Thus, the *side* pathway requires 7–8 kcal/mol less energy than the *bottom* pathway to reorganize. Regarding the interaction contribution  $\Delta E_{int}$ , the obtained energy values indicate that the *Side-DD* mechanism is more stable than in *Bottom-BF*. Comparing these contributions energies in both catalysts ( $\Delta E_{reorg\ t}$  versus  $\Delta E_{int}$ ), we find that the interaction energy is greater in the *side* mechanism than the reorganization energy. Consequently, it is reported that in the limiting stage of the *Side-DD* mechanism, the electronic effects predominate over the steric ones, whereas in *Bottom-BF*, the converse is true. Thus, the electronic contributions are accountable for the *Z*-selectivity's stability.

**Table 1.**  $\Delta E^\ddagger$ ,  $\Delta E_{reorg\ t}$  and  $\Delta E_{int}$  for the determinant step of the CM reaction of propene using the Keitz-Grubbs-substituted complexes, Ru-1 and Ru-2. Values are in kcal/mol.

Catalysts	Mechanism	$\Delta E^\ddagger$	$\Delta E_{reorg\ t}$	$\Delta E_{int}$
Ru-1 	<i>Bottom-BF</i> TSCR	8.7	50.9	−42.1
	<i>Side-DD</i> TSCR	−5.7	41.5	−47.1
Ru-2 	<i>Bottom-BF</i> TSCA	3.5	48.9	−45.3
	<i>Side-DD</i> TSCR	−6.2	41.2	−47.5

## 2.2. Bottom and Side DFT Mechanism Using Novel Ruthenium Catalysts, Ru-7 to Ru-10

In Tables 2 and 3, the energies of intermediates and transition states associated with the *Bottom* and *Side* pathways of the CM utilizing Ru-7 to Ru-10 catalysts are listed. The *Side-DD* demonstrates low energy barriers, indicating that thermal equilibrium could be readily achieved in all catalysts. In particular, the TSCR with Gibbs energies ( $\Delta G^\ddagger$ ) between 16.4–17.4 kcal/mol is the limiting stage. Optimized structures are depicted in Figure S5–S8. For the *Bottom-BF*, the limiting stage is the TSCA in the Ru-8 and Ru-10 with  $\Delta G^\ddagger$  values of 28.6 kcal/mol and 33.4 kcal/mol, respectively. In Ru-7 and Ru-9, the TSCR has a  $\Delta G^\ddagger$  of 33.3 kcal/mol. Consequently, these results are comparable to those of Ru-1 and Ru-2, indicating that Ru-7 to Ru-10 are active and stable catalysts for the production of *Z*-alkenes.

In addition, Table 4 displays the difference in the barrier Gibbs energy between the two mechanisms  $\Delta\Delta G_{Bottom-Side}$  for Ru-7 to Ru-10. The minimum value reported is 11.2 kcal/mol for the Ru-8 catalyst, while the utmost is 19.3 kcal/mol for the Ru-10 catalyst. These results demonstrate the *Side* preference of these catalysts, which is consistent with what has been reported for comparable complexes [32]

**Table 2.** Gibbs energy values (kcal/mol) of the intermediates and transition states connected to the *Bottom-BF* mechanism of Ru-7 to Ru-10 catalysts.

Catalyst	CA	TSCA	MC-I	TSMC	MC-II	TSCR	DSCA
Ru-7	3.5	31.0	20.9	23.9	21.8	33.3	17.0
Ru-8	0.6	28.6	17.7	27.4	17.0	27.6	12.0
Ru-9	4.3	32.8	23.2	26.2	22.8	33.3	17.0
Ru-10	1.7	33.4	19.9	23.5	18.7	29.3	13.2

**Table 3.** Gibbs energy values (kcal/mol) of the intermediates and transition states connected to the *Side-DD* mechanism of Ru-7 to Ru-10 catalysts.

Catalyst	CA	TSCA	MC-I	TSMC	MC-II	TSCR	DSCA
Ru-7	2.6	12.8	0.0	9.5	2.9	17.4	12.4
Ru-8	1.2	13.5	0.0	9.5	3.1	17.4	10.0
Ru-9	5.4	15.3	0.0	12.4	1.7	16.8	12.6
Ru-10	0.5	13.5	0.6	10.4	2.5	16.4	7.3

**Table 4.** Difference in the barrier Gibbs energy  $\Delta\Delta G_{\text{Bottom-Side}}$  between Ru-7 and Ru-10 catalysts. Values are in kcal/mol.

Catalyst	$\Delta\Delta G_{\text{Bottom-Side}}$
Ru-7	15.9
Ru-8	11.2
Ru-9	16.6
Ru-10	19.3

### 2.3. Side Mechanism and Analysis of the Electronic and Steric Role in Recent Z-Selective Catalysts (Ru-1, Ru-7, and Ru-9) Containing a Carboxylate as Anionic Group

Figure 5 depicts the profile energy of cross metathesis utilizing Ru-1, Ru-7, and Ru-9 to compare the role of bulky ligands (Mes, Dipp, and Dipep) when a carboxylate group is used as an auxiliary ligand. Ru-7 catalysts are the most stable thermodynamically in the initial stages of the mechanism, followed by Ru-1 and Ru-9. However, when the MC-II is formed and [2+2] cycloreversion occurs, the stability order changes to Ru-9 > Ru-7 > Ru-1 (Dipep > Dipp > Mes), showing barrier energies of 18.4 kcal/mol for Ru-1, 17.4 kcal/mol for Ru-7 and 16.8 kcal/mol for Ru-9.

The energetic values corresponding to the steric and electronic contributions to the determinant step are displayed in Table 5. The binding energy ( $\Delta E^{\ddagger}$ ) for Ru-1, Ru-7, and Ru-9 is  $-5.7$  kcal/mol,  $-6.9$  kcal/mol, and  $-6.6$  kcal/mol, respectively. The results indicated that  $\Delta E^{\ddagger}$  is favored using bulky ligands. Additionally, reorganization ( $\Delta E_{\text{reorg } t}$ ) and interaction ( $\Delta E_{\text{int}}$ ) energies exhibit a trend like the obtained in the binding energy, demonstrating that the volume of the ligand has a significant impact on the bond energy contributions. Specifically, it can be observed that Ru-9 has a greater 14e- fragment reorganization ( $\Delta E_{\text{reorg } 14e}$ ) than Ru-7 and Ru-1. Regarding  $\Delta E_{\text{int}}$ , Ru-1 and Ru-7 catalysts exhibit comparable values,  $-47.0$  kcal/mol and  $-47.6$  kcal/mol, respectively, whereas Ru-9 is  $-50.9$  kcal/mol. This result indicates that Ru-9 (Dipep) has the lowest interaction energy. Furthermore, if we compare the total reorganization energy contribution to that of the interaction, we find that the former is less than the latter. Therefore, the electronic contributions are more prominent than the steric contributions at the mechanism's limiting stage.

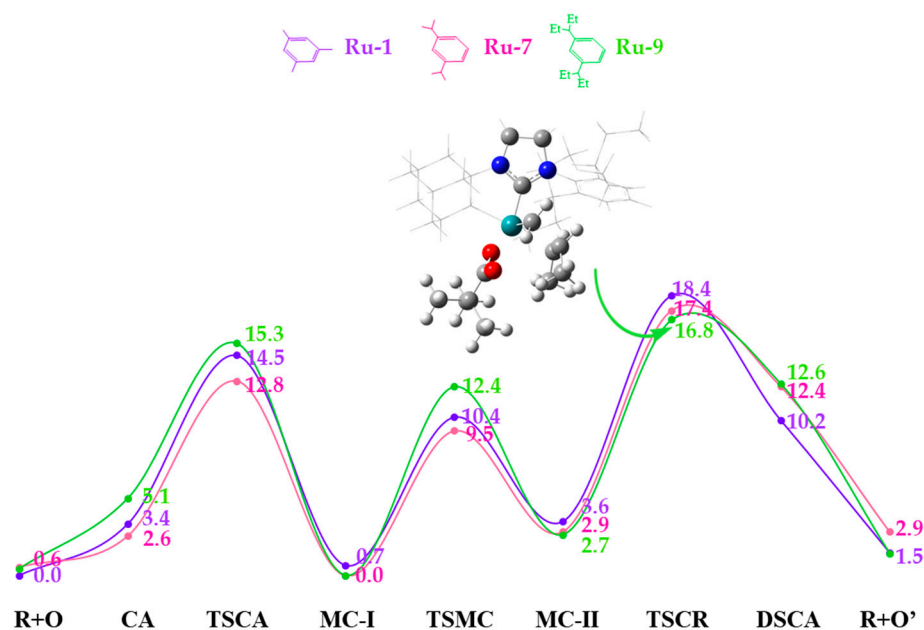


**Figure 5.** Profile of Gibbs energy for the CM reaction of propene with Ru-1, Ru-7, and Ru-9 via *Side-DD*. Values are in kcal/mol.

**Table 5.**  $\Delta E^\ddagger$ ,  $\Delta E_{reorg\ t}$ , and  $\Delta E_{int}$  for the determinant step of the CM reaction of propene using Ru-1, Ru-7, and Ru-9. Values are in kcal/mol.

Catalyst	$\Delta E^\ddagger$	$\Delta E_{reorg\ t}$	$\Delta E_{reorg\ olef}$	$\Delta E_{reorg\ 14e}$	$\Delta E_{int}$
Ru-1	−5.7	41.5	20.1	21.4	−47.1
Ru-7	−6.9	40.7	19.1	21.6	−47.6
Ru-9	−6.6	44.3	20.9	23.4	−50.9

#### 2.4. Side Mechanism and Analysis of the Electronic and Steric Role in Recent Z-Selective Catalyst (Ru-2, Ru-8, and Ru-10) with Nitrate as Anionic Group

Figure 6 depicts the profile energy of cross-metathesis using Ru-2, Ru-8, and Ru-10. This study compares the role of bulky ligands (Mes, Dipp, and Dipep) when the nitrate group is employed as an auxiliary ligand. In general, the thermodynamic stability of the pathways involving the catalysts Ru-8 and Ru-10 is greater than that of Ru-2.

Nevertheless, when the determinant step was analyzed in detail,  $\Delta G^\ddagger$  values of 16.0 kcal/mol, 17.4 kcal/mol, and 16.4 kcal/mol were determined for Ru-2, Ru-8, and Ru-10, respectively. This trend is the inverse of what was observed for Ru-1 (Mes), Ru-7 (Dipp), and Ru-9 (Dipep), in which the highest barrier energy was reached for the catalyst with less bulky ligand Ru-1.

Table 6 displays the results of the EDA with Ru-2, Ru-8 and Ru-10 catalysts. The bond energy ( $\Delta E^\ddagger$ ) is −6.2 kcal/mol, −7.5 kcal/mol, and −13.3 kcal/mol, respectively, which increased in correlation with the steric demand of the lateral NHC. Regarding the contribution of reorganization ( $\Delta E_{reorg\ t}$ ) and interaction energy ( $\Delta E_{int}$ ), the latter is greater than the former, similar to Ru-1, Ru-7, and Ru-9, emphasizing the importance of the electronic effect over the steric effect in the determinant stage. Specifically, the interaction energy for Ru-10 is 8.4 and 7.0 kcal/mol more stable than Ru-8 and Ru-2, respectively. On the other hand, the values of  $\Delta E_{reorg\ 14e}$  show that this contribution decreases with the increase of the bulky ligand, which is opposite to Ru-1, Ru-7, and Ru-9. Specifically, the Ru-10 catalyst exhibits a decrease of 2.4 and 1.4 kcal/mol in comparison to the Ru-2 and Ru-8 catalysts, respectively. This lower reorganization energy for the 14e- fragment is compensated by an increase of 2.8 kcal/mol in the reorganization energy of the olefin. Therefore, despite the fact that the barrier energies for Ru-9 and Ru-10 are similar and are controlled by the interaction energy, the steric effects are different due to the nature of the auxiliary ligand.

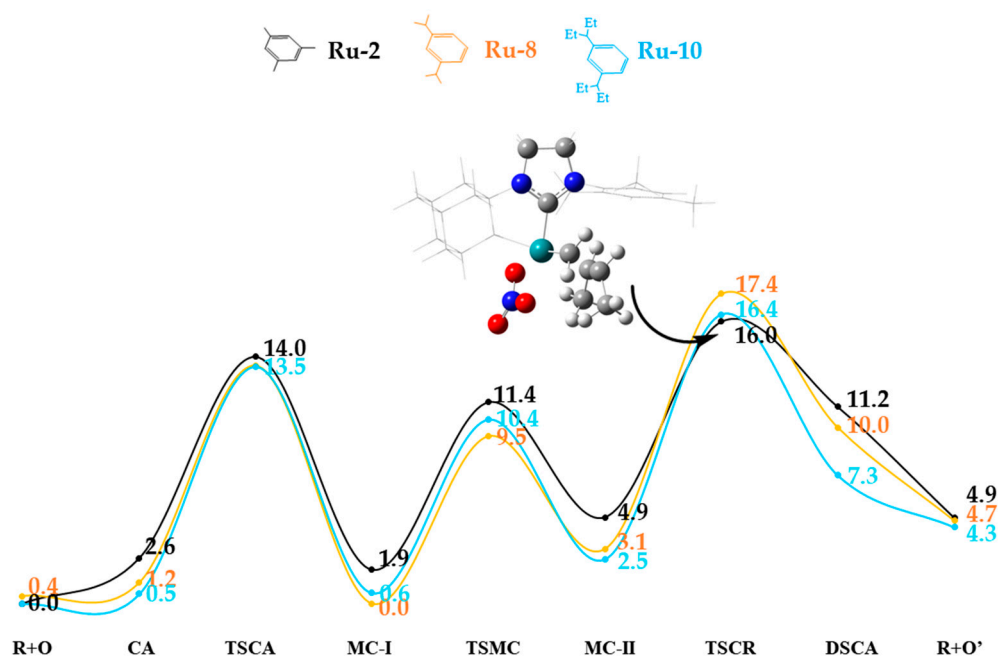


**Figure 6.** Profile of Gibbs energy for the CM reaction of propene with Ru-2, Ru-8, and Ru-10 via *Side-DD*. Values are in kcal/mol.

**Table 6.**  $\Delta E^\ddagger$ ,  $\Delta E_{reorg\ t}$ , and  $\Delta E_{int}$  for the determinant step of the CM reaction of propene using Ru-2, Ru-8, and Ru-10. Values are in kcal/mol.

Catalyst	$\Delta E^\ddagger$	$\Delta E_{reorg\ t}$	$\Delta E_{reorg\ olef}$	$\Delta E_{reorg\ 14e}$	$\Delta E_{int}$
Ru-2	−6.2	41.2	20.0	21.2	−47.5
Ru-8	−7.5	38.6	18.4	20.2	−46.1
Ru-10	−13.3	40.0	21.2	18.8	−54.5

To gain a better understanding of why Ru-10 has a lower steric effect than Ru-8, the optimized structures of the transition state were analyzed. According to Figure 7, it can be noted that in the Ru-8 catalyst, the Dipp *side* arm is located at 3.646 Å from the olefin, forming an angle dihedral of Ru-C1-N-C2 of 20.7° and an angle C1-Ru-C(olefin) of −6.9°. However, this distance is greater for the Ru-10 complex, being 3.720 Å and the dihedral angles and angle are 35.7° and −11°, respectively. These results show that in Ru-10, both the *side* arm and the olefin adopt favorable orientations for sterically decongesting the cycloreversion reaction. Therefore, the repulsive forces between the *side* arm and the olefin are stronger with the Dipep compared to Dipp groups (Dipp <<<< Dipep).

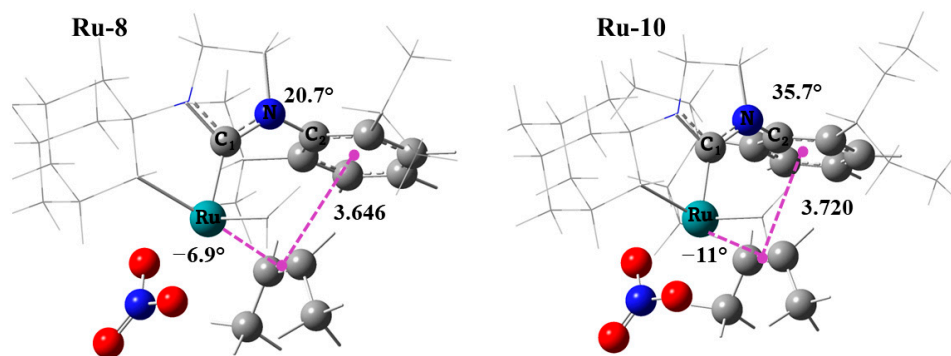


**Figure 7.** Optimized geometry of the TSCR for Ru-8 and Ru-10 in the mechanism *Side-DD*. Distances are given in Å.

### 3. Discussion

According to the preceding, a distinct behavior is observed when pivalate and nitrate are used as auxiliary ligands. For instance, the barrier energies  $\Delta G^\ddagger$  increase when the bulky ligand is greater if the auxiliary ligand is a nitrate and decrease when the auxiliary ligand is pivalate. This result is consistent with the report by Grubbs and co-workers [22]. Ru-7 (nitrate ligand) produces more Z-olefin than Ru-8 (pivalate ligand). Moreover, the interaction energies between Ru-1 and Ru-2, as well as Ru-9 and Ru-10, exhibit greater favorability in Ru-2 and Ru-10, respectively, owing to the inclusion of the nitrate ligand.

These differences can be explained by the fact that Ru-10 exhibited the lowest reorganization energy  $\Delta E_{reorg\ 14e}$  when compared to Ru-2 and Ru-8, suggesting that in the presence of the nitrate ligand, a rearrangement occurs more easily despite the presence of the bulky ligands. Nevertheless, for the catalysts Ru-1, Ru-7, and Ru-9 with carboxylate as an auxiliary ligand, a higher reorganization energy  $\Delta E_{reorg\ 14e}$  is found when there are bulky ligands, as should be expected. Thus, the structural reorganization as energy that controls the reactivity in olefin metathesis has also been observed in Mo catalysts [39], in 1st- and 2nd-generation Grubbs catalysts [30] and currently, in RCM utilizing 2nd-Grubbs catalysts, where the much larger distortion disfavors the olefin coordination [40]. Table 7 presents a summary of these results.

**Table 7.** Summary of the most significant results. Values are in kcal/mol.

<i>t</i> -BuCOO <sup>−</sup>	$\Delta G^\ddagger$	$\Delta E_{reorg\ 14e}$	NO <sub>3</sub> <sup>−</sup>	$\Delta G^\ddagger$	$\Delta E_{reorg\ 14e}$
Ru-1: Mes	18.4	21.4	Ru-2: Mes	16.0	21.2
Ru-7: Dipp	17.4	21.6	Ru-8: Dipp	17.0	20.2
Ru-9: Dipep	16.8	23.4	Ru-10: Dipep	16.4	18.8

This nitrate behavior difference can be explained by a strong electronic interaction generated between an oxygen coming from the auxiliary group and one of the substituted hydrogens of the auxiliary olefin (O---H). Figure 8 illustrates the optimized structure of the limiting stage of Ru-9 and Ru-10 catalysts to demonstrate the existence of this effect. The O---H interaction lengths in the Ru-9 and Ru-10 catalyst are 2.619 Å and 2.584 Å, respectively. Therefore, the system containing nitrate ligand presents a distance smaller O---H than the carboxylate ligand, which demands low reorganization energy and demonstrates the possible existence of a “nitrate effect”. Importantly, this analysis was also carried out and observed with the other catalysts Ru-1 versus Ru-2 and Ru-7 versus Ru-8, as shown in Figures S9 and S10 of the Supplementary Material (SM), respectively.

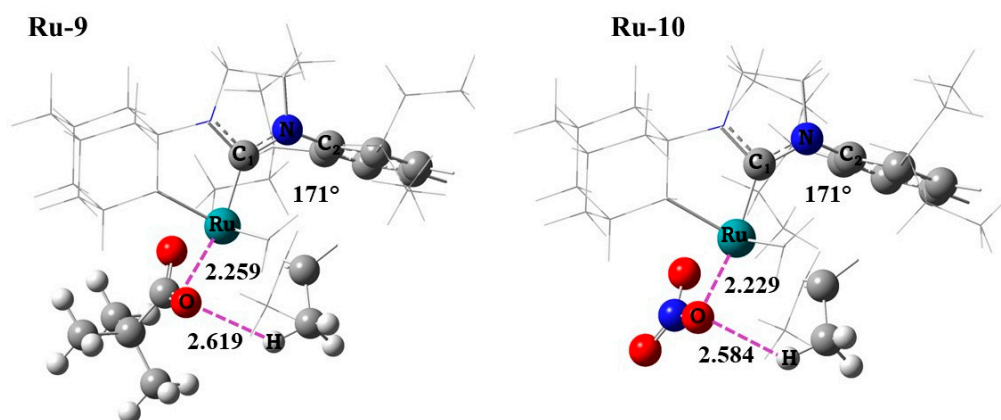


**Figure 8.** Optimized geometry of the TSCR for Ru-9 and Ru-10 in the mechanism *Side-DD*. Distances are expressed in Å.

Moreover, another outstanding result is the fact that the interaction energy is slightly higher than the reorganization energy, suggesting that both contributions are crucial for

understanding the reactivity of these systems. We quantify the steric congestion into Z-selective ruthenium catalysts using the steric maps of Cavallo and co-workers [41] (Figure 9). The steric maps disclose that these catalysts have high steric hindrance ( $\%V_{bur}$ ), where it reached a minimum limit of 68.3% with the Ru-2 catalyst and a maximum of 75.9% with the Ru-9 catalyst. These percentages are substantially greater than those obtained with the Hoveyda–Grubbs catalyst (Figure S11 and Tables S1 and S2 of the supplementary material). The results show that if the carboxylate ligand is used as an anionic group, an increase in the steric hindrance ( $\%V_{bur}$ ) of 72, 74.8, and 75.9% for Ru-1, Ru-7, and Ru-9, respectively. In contrast, when the nitrate ligand is present, the  $\%V_{bur}$  decreases to 68.3, 70.6, and 72.0% in Ru-2, Ru-8, and Ru-10, respectively. Additionally, it is essential to analyze the free volume ( $\%V_{free}$ ). It can be associated with the free space required for the formation of the new *cis*-olefin (Tables S3–S6 of the supplementary material). The results show a  $\%V_{free}$  of 28, 31.7, 25.2, 29.4, 24.1 and 28.0 for Ru-1, Ru-2, Ru-7, Ru-8, Ru-9 and Ru-10, respectively. These results show that the larger free volume occurs in Ru-2 and Ru-8. Thus, the use of nitrate and Dipp as auxiliary and bulky ligands in a Ru catalyst can result in a higher free volume. Consequently, nitrate ligands allow a larger free volume than carboxylate, which is associated with the catalytic superiority of the nitrate complexes over the substituted tertiary butyls.

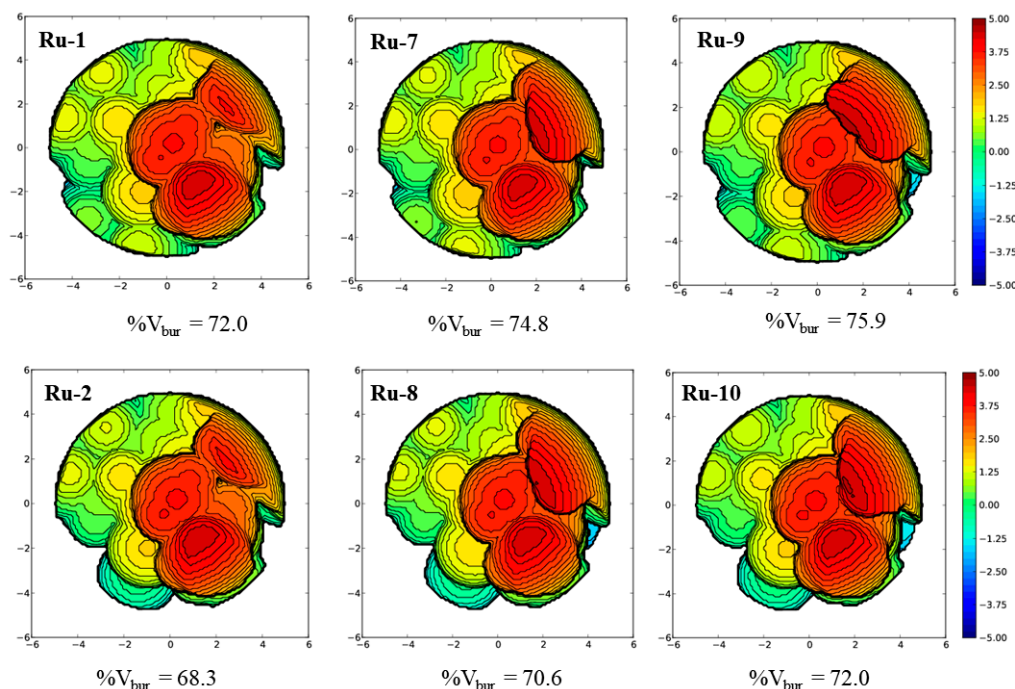


**Figure 9.** Topographic steric maps of ruthenium catalysts in the determinant stage of the reaction mechanism.

To complement the discussion, an analysis of the charge distribution in the determining step, the [2+2] cycloreversion, was performed for each of the studied catalysts Ru-1, Ru-2; Ru-7, Ru-8, and Ru-9, Ru-10, with Mes, Dipp, and Dippep as the NHC ligand arms, respectively. Table 8 displays the results for each system considering the charge associated with the central atom ( $Q_{Ru}$ ), to anionic auxiliary ligand ( $Q_{Anionic}$ ), to the NHC ligand ( $Q_{NHC}$ ), to the adamant group ( $Q_{Adm}$ ), the carbene bond ( $Q_{carbene}$ ), and the olefin ( $Q_{olefin}$ ). The results reveal that the auxiliary ligand and the carbene bond are electron acceptors, whereas the rest of the molecule has an electron donor character. Specifically, the charge distribution in  $Q_{Anionic}$  is observed to be greater with nitrate than with carboxylate ligands. The charge associated with the carbene bond  $Q_{carbene}$  exhibits the opposite trend, with greater electron acceptor character in catalysts containing carboxylate. In addition, the ruthenium atom is a strong charge donor, whereas NHC, adamantly and the olefin are weak

charge donors. Importantly, the charge distribution is independent of the steric influence that contributes to the arm NHC ligand (L = Mes, Dipp, Dipep). However, as was observed in Ru-2 (0.108), Ru-8 (0.081), and Ru-10 (0.027), the donor character in the olefin ( $Q_{olefin}$ ) decreases with the presence of a bulky ligand. Therefore, the exceptional characteristics of catalysts with nitrate ligand, such as the highest electron acceptor behavior and the lowest reorganization energy, are a result of a combination of electronic and steric effects.

**Table 8.** Atomic charges (Q) associated with the stabilizing ligands and the metal fragment.

Catalysts	$Q_{Anionic}$	$Q_{Ru}$	$Q_{Carbene}$	$Q_{NHC}$	$Q_{olefin}$	$Q_{Adm}$
Ru-1	−0.497	0.509	−0.187	0.032	0.078	0.065
Ru-2	−0.640	0.537	−0.119	0.011	0.108	0.103
Ru-7	−0.487	0.541	−0.192	0.017	0.059	0.062
Ru-8	−0.617	0.614	−0.164	0.010	0.081	0.076
Ru-9	−0.503	0.548	−0.193	0.017	0.071	0.060
Ru-10	−0.605	0.574	−0.179	0.022	0.027	0.161

## 4. Materials and Methods

### 4.1. Models

The studied catalysts were divided into two groups, as shown in Figure 10. The first group consists of the active species (14-Int), so-called Keitz–Grubbs-substituted complexes. These complexes are characterized by the presence of an NHC with a Mes substituent and bidentate anionic ligands, such as tert-butyl (Ru-1) and nitrate (Ru-2). The second group includes the active species of complexes reported by Grubbs et al. in 2020. These systems incorporate the bulky lateral arms of Dipp and Dipep. The catalysts are denoted as Ru-7 (L = Dipp, t-Bu-C); Ru-8 (L = Dipp, O-N<sup>+</sup>); Ru-9 (L = Dipep, t-Bu-C); and Ru-10 (L = Dipep, O-N<sup>+</sup>). It is important to highlight that Ru-10 is a proposed catalyst because computational and experimental efforts have shown that the inclusion of the nitrate group in conventional catalysts has significantly improved *Z*-selectivity [17].

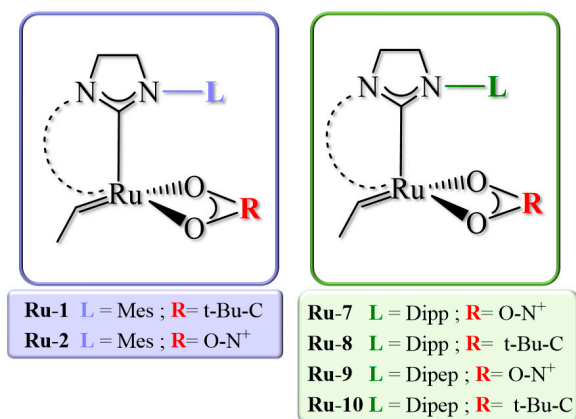


**Figure 10.** Active species used in this work.

The active catalytic species (14-Int) of the catalysts were chosen based on the findings reported by Núñez-Zarur and co-workers [42]. According to his research, the formation of this intermediate in the second-generation Hoveyda–Grubbs precatalysts occurs by a dissociative mechanism, primarily driven by the kinetic preference for the elimination of the alkoxy group. Thus, with Hoveyda-Grubbs catalysts, the initiation step involves (a) the loss of the chelating alkoxy group and (b) a cross-metathesis process in which the initial substituent of the active species is exchanged for the substituent of the reactive alkene. The preceding was depicted in Figure S12 of the Supplementary material.

#### 4.2. Computational Details

Density Functional Theory (DFT) was used as it is implemented in Gaussian-16 software. All molecular structures were optimized in the gas phase using the meta-GGA-type functional M06-L. This function has been previously studied for the Grubbs catalysts because it includes attractive non-covalent interactions that are determinants for an accurate energy description [43,44]. The electronic configuration of the ruthenium atom combines the MWB28 [45,46] pseudopotential, which replaces the inner electrons with a non-local effective potential, and the (8s7p6d)/[6s5p3d] basis set to describe the valence electrons. The 6-31 + G(d, p) basis set was utilized to represent carbon, hydrogen, oxygen, and nitrogen atoms. To ensure the nature of each structure as an intermediate or transition state on the potential energy surfaces (PES), a vibrational analysis of all stationary points was performed by calculating the Hessian matrix in internal coordinates (second derivative of the energy with respect to position). These frequencies were used to determine the thermal contributions to enthalpy (H) and Gibbs free energy (G) utilizing the harmonic oscillator and rigid rotor model implemented in Gaussian-16 and assuming a temperature of 298 K at standard pressure (1 atm). The effects of the tetrahydrofuran (THF) solvent were included with the density-based solvation model (SMD) [45,46] as energetic corrections from single-point calculations. In summary, the reported Gibbs free energy for each species in the PES was obtained by  $G = G_{\text{opt}} + G_{\text{solv}}$ .

#### 4.3. Theoretical Background

##### 4.3.1. Energy Decomposition Analysis (EDA)

The energy decomposition analysis allows us to understand the changes of a chemical process through the equation proposed by Houk [47] to quantitatively assess binding energy ( $E^\ddagger$ ). This model has been successfully used for olefin metathesis reactions in Molybdenum and Ruthenium complexes [39,48]. The binding energy of the determinant step into the mechanism may be comprehended by considering two distinct contributions. These can be attributed to the rearrangement  $\Delta E_{\text{reorg total}}$  and the interaction energy  $\Delta E_{\text{int}}$  between the metal fragment and the olefin. The former is related to the steric effect, while the latter is associated with the electronic influence. The energy partitioning from the energy barrier ( $E^\ddagger$ ) is defined as

$$\Delta E^\ddagger = \Delta E_{\text{reorg total}} + \Delta E_{\text{int}}$$

$\Delta E_{\text{reorg total}}$  analyzes the changes in the geometry of the active species  $\Delta E_{\text{reorg 14}}$  and of the olefin  $\Delta E_{\text{reorg olefin}}$  allowing the degree of structural distortion between the fundamental state and the distorted state to be quantified so that:

$$\begin{aligned} \Delta E_{\text{reorg total}} &= \Delta E_{\text{reorg 14}} + \Delta E_{\text{reorg olefin}} \\ &= \left( E_{14 \text{ e-atcomplex}} - E_{14 \text{ e-reactive}} \right) + \left( E_{\text{olefin at complex}} - E_{\text{olefin}} \right) \end{aligned}$$

The interaction energy is then obtained using the results of  $\Delta E^\ddagger$  and  $\Delta E_{\text{reorg total}}$ :

$$\Delta E_{\text{int}} = \Delta E^\ddagger - \Delta E_{\text{reorg total}}$$

##### 4.3.2. Topographic Maps

The application of topographic steric maps has been extremely useful in the design of transition metal complexes [25,38,49,50]. The computational tool developed by Carvallo et al. [41] provides a picture of the interaction surface between the catalyst and the substrates that are formed by the ligands in the complex. The steric hindrance of the above catalysts in the limiting stage has been represented using topographic maps through a comparative analysis of the buried volume (% $V_{\text{bur}}$ ); the preceding was interpreted [51]. The orientation of the map was adjusted to avoid steric interference from NHC *side* arms. The Ru atom was defined to be located at the origin, while the Ru-alkylidene resides on the z+ axis, and

the bulk-type ligand lies in the *xy* plane. (Figure S13) The radius of the sphere surrounding the center of the metal was set to 5.0 Å [52,53]. (Figure S11) For the other atoms, the Bondi radii were scaled by 1.17, and a mesh of 0.1 Å was selected to scan the sphere for buried voxels. H atoms were included in the calculations.

## 5. Conclusions

This study investigates the impact of bulky ligands (L = Mes, Dipp, and Dippep) on novel sterically demanding N-heterocyclic cyclometalated ruthenium complexes. Nitrate and pivalate are employed as auxiliary ligands to understand the underlying factors contributing to the *Z*-selectivity in cross-metathesis reactions. Our results reveal the Side preference in the reaction mechanism indicated by the difference in Gibbs energy barriers  $\Delta\Delta G_{\text{Bottom-Side}}$  ranging from 11.2–19.3 kcal/mol. The [2+2] cycloreversion was identified as the rate-determinant step, showing comparable energy values in all the catalysts. However, it has been shown that the activation energies  $\Delta G^\ddagger$  exhibit an increase as the size of the bulky ligand increases in catalysts, including nitrate as an auxiliary ligand. Conversely, the energies display a decrease when pivalate is employed as the auxiliary ligand. This difference can be attributed to the relatively low reorganization energy required for a rearrangement in the coordination environment. This is further evidenced by the short O---H distance between the oxygen atom of the auxiliary ligand and the hydrogen atom of the olefin. Moreover, the results also explain that the rate-determinant step is not just influenced by steric effects but also by electronic factors coming from the electron acceptor character of the auxiliary ligand and the donor characteristics of the ruthenium atom.

**Supplementary Materials:** The following supplementary material information can be downloaded at: <https://www.mdpi.com/article/10.3390/catal13091305/s1>, Figures S1 and S2: Gibbs profile energies of catalysts Ru-1 and Ru-2. Figures S3–S8: Geometry of the optimized structures associated to Ru-1, Ru-2, Ru-7, Ru-8, Ru-9 and Ru-10. Figure S9: Optimized geometry of the TSCR of the Ru-1 and Ru-2 catalysts. Figure S10: Optimized geometry of the TSCR of the Ru-7 and Ru-8 catalysts. Figure S11: Radius of the sphere built around Ru-1. Figure S12: Dissociation mechanism in Hoveyda-Grubbs catalysts. Figure S13: Visualization of the orientation used in steric maps with the Ru-1 catalyst. Table S1: Values of %V<sub>free</sub> and %Buried for Ru-1; Table S2: Values of %V<sub>free</sub> and %Buried for Ru-2; Table S3: Values of %V<sub>free</sub> and %Buried for Ru-7; Table S4: Values of %V<sub>free</sub> and %Buried for Ru-8; Table S5: Values of %V<sub>free</sub> and %Buried for Ru-9; Table S6: Values of %V<sub>free</sub> and %Buried for Ru-10; Cartesian coordinates of the structure optimized by DFT.

**Author Contributions:** Conceptualization, K.P.-G.; methodology, K.P.-G. and V.D.-G.; formal analysis, V.D.-G. and K.P.-G.; investigation V.D.-G.; writing—original draft preparation, K.P.-G. and V.D.-G. All authors have read and agreed to the published version of the manuscript.

**Funding:** This research was funded by ANID through FONDECYT project 11200264 and ANID + InES Género+ INGE210029. K.Paredes-Gil acknowledges the computational resources provided by the high-performance computing system of PIDi-UTEM (SCC-PIDi-UTEM FONDEQUIP-EQM180180), and the supercomputing infrastructure of the NLHPC (ECM-02).

**Data Availability Statement:** Not applicable.

**Conflicts of Interest:** The authors declare no conflict of interest.

## References

1. Turczel, G.; Kovács, E.; Merza, G.; Coish, P.; Anastas, P.T.; Tuba, R. Synthesis of Semiochemicals via Olefin Metathesis. *ACS Sustain. Chem. Eng.* **2019**, *7*, 33–48. [CrossRef]
2. Eivgi, O.; Guidone, S.; Frenklah, A.; Kozuch, S.; Goldberg, I.; Lemcoff, N.G. Photoactivation of Ruthenium Phosphite Complexes for Olefin Metathesis. *ACS Catal.* **2018**, *8*, 6413–6418. [CrossRef]
3. Biermann, U.; Bornscheuer, U.T.; Feussner, I.; Meier, M.A.R.; Metzger, J.O. Fatty Acids and Their Derivatives as Renewable Platform Molecules for the Chemical Industry. *Angew. Chem.—Int. Ed.* **2021**, *60*, 20144–20165. [CrossRef]
4. Nieniałowski, T.; Krzesiński, P.; Baumert, M.E.; Skoczeń, A.; Suska-Kauf, E.; Pawłowska, J.; Kajetanowicz, A.; Grela, K. 4-Methyltetrahydropyran as a Convenient Alternative Solvent for Olefin Metathesis Reaction: Model Studies and Medicinal Chemistry Applications. *ACS Sustain. Chem. Eng.* **2020**, *8*, 18215–18223. [CrossRef]

5. Gawin, R.; Czarnecka, P.; Grela, K. Ruthenium Catalysts Bearing Chelating Carboxylate Ligands: Application to Metathesis Reactions in Water. *Tetrahedron* **2010**, *66*, 1051–1056. [[CrossRef](#)]
6. Herbert, M.B.; Grubbs, R.H. Z-Selective Cross Metathesis with Ruthenium Catalysts: Synthetic Applications and Mechanistic Implications. *Angew. Chem.—Int. Ed.* **2015**, *54*, 5018–5024. [[CrossRef](#)]
7. Hughes, D.L. Highlights of the Recent U.S. Patent Literature: Focus on Metathesis. *Org. Process Res. Dev.* **2016**, *20*, 1008–1015. [[CrossRef](#)]
8. Patrick Montgomery, T.; Johns, A.M.; Grubbs, R.H. Recent Advancements in Stereoselective Olefin Metathesis Using Ruthenium Catalysts. *Catalysts* **2017**, *7*, 87. [[CrossRef](#)]
9. Paredes-Gil, K.; Sivasamy, R.; Mendizábal, F. A Mechanistic DFT Study of Z-Selective Ring-Opening Metathesis Polymerization by MAP Catalysts. *Mol. Catal.* **2022**, *527*, 112418. [[CrossRef](#)]
10. Sousa-Silva, A.; Paredes-Gil, K.; De Matos, J.M.E.; Sá, É. Singlet Spin State Drives [V]-Carbene to Catalyze Olefin Metathesis: A Computational Analysis. *Organometallics* **2022**, *41*, 1295–1303. [[CrossRef](#)]
11. Peryshkov, D.V.; Schrock, R.R.; Takase, M.K.; Müller, P.; Hoveyda, A.H. Z-Selective Olefin Metathesis Reactions Promoted by Tungsten Oxo Alkylidene Complexes. *J. Am. Chem. Soc.* **2011**, *133*, 20754–20757. [[CrossRef](#)] [[PubMed](#)]
12. Ogba, O.M.; Warner, N.C.; O’Leary, D.J.; Grubbs, R.H. Recent Advances in Ruthenium-Based Olefin Metathesis. *Chem. Soc. Rev.* **2018**, *47*, 4510–4544. [[CrossRef](#)] [[PubMed](#)]
13. Keitz, B.K.; Endo, K.; Herbert, M.B.; Grubbs, R.H. Z -Selective Homodimerization of Terminal Olefins with a Ruthenium Metathesis Catalyst. *J. Am. Chem. Soc.* **2011**, *133*, 9686–9688. [[CrossRef](#)] [[PubMed](#)]
14. Wang, T.; Yu, X.; Zhang, H.; Wu, S.; Guo, W.; Wang, J. Synthesis and Evaluation of Ruthenium 2-Alkyl-6-Mercaptophenolate Catalysts for Olefin Metathesis. *Appl. Organomet. Chem.* **2019**, *33*, 4939. [[CrossRef](#)]
15. Dawood, K.M.; Nomura, K. Recent Developments in Z-Selective Olefin Metathesis Reactions by Molybdenum, Tungsten, Ruthenium, and Vanadium Catalysts. *Adv. Synth. Catal.* **2021**, *363*, 1970–1997. [[CrossRef](#)]
16. Grzesiński, Ł.; Milewski, M.; Nadirova, M.; Kajetanowicz, A.; Grela, K. Unexpected Latency of Z-Stereoretentive Ruthenium Olefin Metathesis Catalysts Bearing Unsymmetrical N-Heterocyclic Carbene or Cyclic(Alkyl)(Amino)Carbene Ligands. *Organometallics* **2022**, *428*. [[CrossRef](#)]
17. Keitz, B.K.; Endo, K.; Patel, P.R.; Herbert, M.B.; Grubbs, R.H. Improved Ruthenium Catalysts for Z-Selective Olefin Metathesis. *J. Am. Chem. Soc.* **2012**, *134*, 693–699. [[CrossRef](#)]
18. Khan, R.K.M.; Torker, S.; Hoveyda, A.H. Readily Accessible and Easily Modifiable Ru-Based Catalysts for Efficient and Z-Selective Ring-Opening Metathesis Polymerization and Ring-Opening/Cross- Metathesis. *J. Am. Chem. Soc.* **2013**, *135*, 10258–10261. [[CrossRef](#)]
19. Koh, M.J.; Khan, R.K.M.; Torker, S.; Yu, M.; Mikus, M.S.; Hoveyda, A.H. High-Value Alcohols and Higher-Oxidation-State Compounds by Catalytic Z-Selective Cross-Metathesis. *Nature* **2015**, *517*, 181–186. [[CrossRef](#)]
20. Rosebrugh, L.E.; Marx, V.M.; Keitz, B.K.; Grubbs, R.H. Synthesis of Highly Cis, Syndiotactic Polymers via Ring-Opening Metathesis Polymerization Using Ruthenium Metathesis Catalysts. *J. Am. Chem. Soc.* **2013**, *135*, 10032–10035. [[CrossRef](#)]
21. Smit, W.; Ekel, J.B.; Occhipinti, G.; Woźniak, B.; Törnroos, K.W.; Jensen, V.R. Z-Selective Monothiolate Ruthenium Indenylidene Olefin Metathesis Catalysts. *Organometallics* **2020**, *39*, 397–407. [[CrossRef](#)]
22. Xu, Y.; Wong, J.J.; Samkian, A.E.; Ko, J.H.; Chen, S.; Houk, K.N.; Grubbs, R.H. Efficient Z-Selective Olefin-Acrylamide Cross-Metathesis Enabled by Sterically Demanding Cyclometalated Ruthenium Catalysts. *J. Am. Chem. Soc.* **2020**, *142*, 20987–20993. [[CrossRef](#)]
23. Ritter, T.; Hejl, A.; Wenzel, A.G.; Funk, T.W.; Grubbs, R.H. A Standard System of Characterization for Olefin Metathesis Catalysts. *Organometallics* **2006**, *25*, 5740–5745. [[CrossRef](#)]
24. Rosebrugh, L.E.; Herbert, M.B.; Marx, V.M.; Keitz, B.K.; Grubbs, R.H. Highly Active Ruthenium Metathesis Catalysts Exhibiting Unprecedented Activity and Z-Selectivity. *J. Am. Chem. Soc.* **2013**, *135*, 1276–1279. [[CrossRef](#)] [[PubMed](#)]
25. Dumas, A.; Tarrieu, R.; Vives, T.; Roisnel, T.; Dorcet, V.; Baslé, O.; Mauduit, M. A Versatile and Highly Z -Selective Olefin Metathesis Ruthenium Catalyst Based on a Readily Accessible N -Heterocyclic Carbene. *ACS Catal.* **2018**, *8*, 3257–3262. [[CrossRef](#)]
26. Małecki, P.; Gajda, K.; Gajda, R.; Woźniak, K.; Trzaskowski, B.; Kajetanowicz, A.; Grela, K. Specialized Ruthenium Olefin Metathesis Catalysts Bearing Bulky Unsymmetrical NHC Ligands: Computations, Synthesis, and Application. *ACS Catal.* **2019**, *9*, 587–598. [[CrossRef](#)]
27. Nelson, J.W.; Grundy, L.M.; Dang, Y.; Wang, Z.X.; Wang, X. Mechanism of Z -Selective Olefin Metathesis Catalyzed by a Ruthenium Monothiolate Carbene Complex: A DFT Study. *Organometallics* **2014**, *33*, 4290–4294. [[CrossRef](#)]
28. Occhipinti, G.; Koudriavtsev, V.; Törnroos, K.W.; Jensen, V.R. Theory-Assisted Development of a Robust and Z-Selective Olefin Metathesis Catalyst. *Dalton Trans.* **2014**, *43*, 11106–11117. [[CrossRef](#)]
29. Nuñez-Zarur, F.; Solans-Monfort, X.; Rodríguez-Santiago, L.; Sodupe, M. Differences in the Activation Processes of Phosphine-Containing and Grubbs-Hoveyda-Type Alkene Metathesis Catalysts. *Organometallics* **2012**, *31*, 4203–4215. [[CrossRef](#)]
30. Paredes-Gil, K.; Jaque, P. Theoretical Characterization of First- and Second-Generation Grubbs Catalysts in Styrene Cross-Metathesis Reactions: Insights from Conceptual DFT. *Catal. Sci. Technol.* **2016**, *6*, 755–766. [[CrossRef](#)]
31. Herbert, M.B.; Suslick, B.A.; Liu, P.; Zou, L.; Dornan, P.K.; Houk, K.N.; Grubbs, R.H. Cyclometalated Z-Selective Ruthenium Metathesis Catalysts with Modified N-Chelating Groups. *Organometallics* **2015**, *34*, 2858–2869. [[CrossRef](#)]

32. Liu, P.; Xu, X.; Dong, X.; Keitz, B.K.; Herbert, M.B.; Grubbs, R.H.; Houk, K.N. Z-Selectivity in Olefin Metathesis with Chelated Ru Catalysts: Computational Studies of Mechanism and Selectivity. *J. Am. Chem. Soc.* **2012**, *134*, 1464–1467. [[CrossRef](#)] [[PubMed](#)]
33. Patra, S.G.; Das, N.K. Recent Advancement on the Mechanism of Olefin Metathesis by Grubbs Catalysts: A Computational Perspective. *Polyhedron* **2021**, *200*, 115096. [[CrossRef](#)]
34. Dang, Y.; Wang, Z.X.; Wang, X. Does the Ruthenium Nitrate Catalyst Work Differently in Z-Selective Olefin Metathesis? A Dft Study. *Organometallics* **2012**, *31*, 8654–8657. [[CrossRef](#)]
35. Sandford, M.S.; Love, J.A.; Grubbs, R.H. Mechanism and Activity of Ruthenium Olefin Metathesis Catalysts. *J. Am. Chem. Soc.* **2001**, *123*, 6543–6554. [[CrossRef](#)]
36. Suresh, C.H.; Koga, N. Orbital Interactions in the Ruthenium Olefin Metathesis Catalysts. *Organometallics* **2004**, *23*, 76–80. [[CrossRef](#)]
37. Montgomery, T.P.; Grandner, J.M.; Houk, K.N.; Grubbs, R.H. Synthesis and Evaluation of Sterically Demanding Ruthenium Dithiolate Catalysts for Stereoretentive Olefin Metathesis. *Organometallics* **2017**, *36*, 3940–3953. [[CrossRef](#)]
38. Martínez, J.P.; Trzaskowski, B. Olefin Metathesis Catalyzed by a Hoveyda-Grubbs-like Complex Chelated to Bis(2-Mercaptoimidazolyl) Methane: A Predictive DFT Study. *J. Phys. Chem. A* **2022**, *126*, 720–732. [[CrossRef](#)]
39. Poater, A.; Solans-Monfort, X.; Clot, E.; Copéret, C.; Eisenstein, O. Understanding D0-Olefin Metathesis Catalysts: Which Metal, Which Ligands? *J. Am. Chem. Soc.* **2007**, *129*, 8207–8216. [[CrossRef](#)]
40. Zhao, F.; Li, Y.; Houk, K.N.; Lu, Q.; Liu, F. Computational Elucidation on the Conformational Control of Selectivity in Intramolecular Ring-Closing Metathesis vs Intermolecular Homometathesis. *J. Org. Chem.* **2023**, *88*, 8512–8521. [[CrossRef](#)]
41. Falivene, L.; Credendino, R.; Poater, A.; Petta, A.; Serra, L.; Oliva, R.; Scarano, V.; Cavallo, L. SambVca 2. A Web Tool for Analyzing Catalytic Pockets with Topographic Steric Maps. *Organometallics* **2016**, *35*, 2286–2293. [[CrossRef](#)]
42. Nuñez-Zarur, F.; Poater, J.; Rodríguez-Santiago, L.; Solans-Monfort, X.; Solà, M.; Sodupe, M. On the Electronic Structure of Second Generation Hoveyda-Grubbs Alkene Metathesis Precursors. *Comput. Theor. Chem.* **2012**, *996*, 57–67. [[CrossRef](#)]
43. Paredes-Gil, K.; Mendizábal, F.; Jaque, P. Further Understanding of the Ru-Centered [2+2] Cycloreversion/Cycloaddition Involved into the Interconversion of Ruthenacyclobutane Using the Grubbs Catalysts from a Reaction Force Analysis. *J. Mol. Model* **2019**, *25*, 305. [[CrossRef](#)] [[PubMed](#)]
44. Paredes-Gil, K.; Solans-Monfort, X.; Rodríguez-Santiago, L.; Sodupe, M.; Jaque, P. DFT Study on the Relative Stabilities of Substituted Ruthenacyclobutane Intermediates Involved in Olefin Cross-Metathesis Reactions and Their Interconversion Pathways. *Organometallics* **2014**, *33*, 6065–6075. [[CrossRef](#)]
45. Ziegler, T.; Autschbach, J. Theoretical Methods of Potential Use for Studies of Inorganic Reaction Mechanisms. *Chem. Rev.* **2005**, *105*, 2695–2722. [[CrossRef](#)]
46. Marenich, A.V.; Cramer, C.J.; Truhlar, D.G. Universal Solvation Model Based on Solute Electron Density and on a Continuum Model of the Solvent Defined by the Bulk Dielectric Constant and Atomic Surface Tensions. *J. Phys. Chem. B* **2009**, *113*, 6378–6396. [[CrossRef](#)]
47. Bickelhaupt, F.M.; Houk, K.N. Das Distortion/Interaction-Activation-Strain-Modell Zur Analyse von Reaktionsgeschwindigkeiten. *Angew. Chem.* **2017**, *129*, 10204–10221. [[CrossRef](#)]
48. Pablo Martínez, J.; Solà, M.; Poater, A. Predictive Catalysis in Olefin Metathesis with Ru-Based Catalysts with Annulated C60 Fullerenes in the N-Heterocyclic Carbenes. *Chem.–A Eur. J.* **2021**, *27*, 18074–18083. [[CrossRef](#)]
49. Arnedo, L.; Chauvin, R.; Poater, A. Olefin Metathesis with Ru-Based Catalysts Exchanging the Typical N-Heterocyclic Carbenes by a Phosphine-Phosponium Ylide. *Catalysts* **2017**, *7*, 85. [[CrossRef](#)]
50. Cruz, T.R.; Masson, G.H.C.; Amorim, K.A.E.; Machado, A.E.H.; Goi, B.E.; Carvalho-Jr, V.P. Ru/Pd Complex and Its Monometallic Fragments as Catalysts for Norbornene Polymerization via ROMP and Addition. *Catalysts* **2022**, *12*, 1111. [[CrossRef](#)]
51. Gómez-Suárez, A.; Nelson, D.J.; Nolan, S.P. Quantifying and Understanding the Steric Properties of N-Heterocyclic Carbenes. *Chem. Commun.* **2017**, *53*, 2650–2660. [[CrossRef](#)] [[PubMed](#)]
52. Troiano, R.; Costabile, C.; Grisi, F. Alternating Ring-Opening Metathesis Polymerization Promoted by Ruthenium Catalysts Bearing Unsymmetrical NHC Ligands. *Catalysts* **2023**, *13*, 34. [[CrossRef](#)]
53. Romero, M.; Macchione, M.A.; Mattea, F.; Strumia, M. The Role of Polymers in Analytical Medical Applications. A Review. *Microchem. J.* **2020**, *159*, 105366. [[CrossRef](#)]

**Disclaimer/Publisher’s Note:** The statements, opinions and data contained in all publications are solely those of the individual author(s) and contributor(s) and not of MDPI and/or the editor(s). MDPI and/or the editor(s) disclaim responsibility for any injury to people or property resulting from any ideas, methods, instructions or products referred to in the content.